Electronic Supplementary Information

A facile synthesis for $BeCl_2$, $BeBr_2$ and BeI_2

Matthias Müller, Florian Pielnhofer and Magnus R. Buchner*

Powder X-ray diffraction

Powder X-ray diffraction was performed with a STOE StadiMP powder diffractometer using Cu-Kα_1 radiation, a Ge monochromator and a Mythen1K detector. Samples were prepared under glovebox atmosphere in Lindemann capillaries of fused silica, which were flame sealed.

RIETVELD refinement

Phase analysis was performed with WinXPOW,[1] profiles were fitted with JANA2006.[2] RIETVELD refinement was carried out with JANA2006 using single crystal data from the literature.[3–5]

IR spectroscopy

The IR spectra were recorded on a BRUKER Alpha II spectrometer with diamond ATR module inside an argon filled glovebox. Processing of the spectra was performed with the OPUS[6] software package and OriginPro8.[7]

Raman spectroscopy

For the Raman spectroscopic measurements a small amount of the respective beryllium halide was collected and flames sealed in boro silicate capillaries with an inner diameter of 0.5 mm. Raman spectra were recorded on a RENISHAW inVia Qontor spectrometer at laser wavelengths of 457 nm, 532 nm, 633 nm and 785 nm and on a RENISHAW inVia Raman microscope at a laser wavelength of 785 nm

DFT calculations

All DFT calculations were carried out with the CRYSTAL14 program package using the PBE+D2 method. The *k*-mesh sampling was 8 x 8 x 8 for all studied compounds and the convergence criterion was set to 10^{-8} Hartree. The applied Basis sets were taken from[8–11]. For the evaluation of the Coulomb and Exchange integrals (TOLINTEG), tolerance factors of 8 8 8 8 and 16 were used. After all full structural optimization including all lattice and atomic site parameters, the IR and Raman active vibrational modes including intensities were calculated. No imaginary frequencies were obtained.

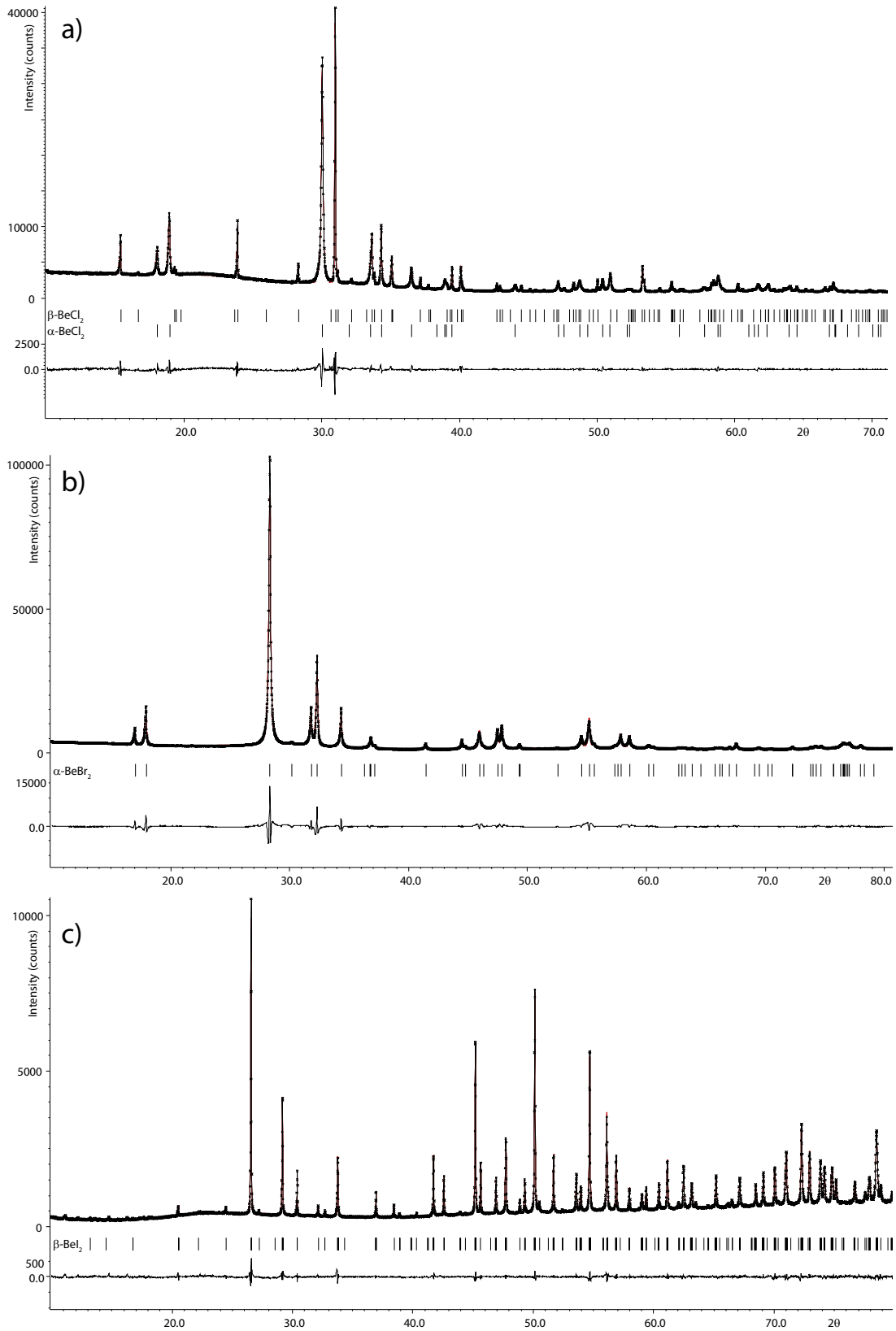

Fig. 1 X-ray powder diffractograms with LeBail profile fit, difference plot and related reference for a) $BeCl_2$ [3,4], b) $BeBr_2$ [5] and c) BeI_2 [5].

Fig. 2 $BeCl_2$ prior to fractionated sublimation.

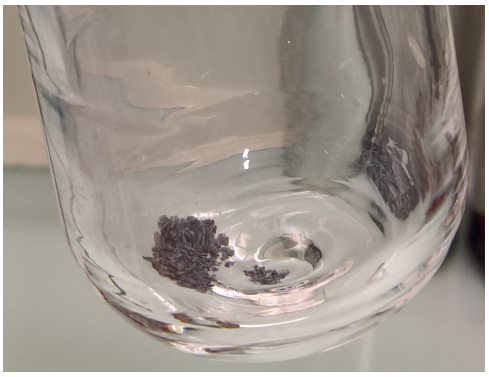

Fig. 3 Unknown lint in the lower part of the ampoule in which $BeCl_2$ was synthesised.

Fig. 4 $BeBr_2$ crystals after sublimation.

Fig. 5 Crystals of BeI_2 at the flame sealed end of the reaction ampule.

Table 1 Experimental and calculated IR and Raman data for BeF_2, $BeCl_2$, $BeBr_2$ and BeI_2.

$\alpha-/\beta-BeF_2$		$\alpha-/\beta-BeCl_2$		$\alpha-BeBr_2$		$\beta-BeI_2$	
IR data / cm^{-1}; experiment (calculated) [mode]							
403	(β: 380) [E_1]	450	(α: 449) [B_{1u}]	404	(400) [B_{1u}]	450	(462)[E_u]
	(α: 388) [E]		(β: 451) [A_{2u}]	416		516	
	(β: 393) [A_2]		(β: 462) [E_u]	462	(492) [B_{2u}]	581	
	(α: 412) [A_2]	583	(α:560) [B_{3u}]	477	(505) [B_{3u}]		
734	(α: 745) [A_2]		(β: 563) [Eu]				
	(α: 747) [E]		(β: 563) [Eu]				
	(β: 754) [E_1]		(β: 569) [A_{2u}]				
	(β: 756) [A_2]		(α: 572) [B_{2u}]				
Raman data / cm^{-1}; experiment (calculated) [mode]							
		174	(α: 169) [B_{3g}]	94	(99) [A_g]	76	(66) [A_{1g}]
			(α: 175) [B_{2g}]	112	(111) [B_{2g}]		(68) [B_{1g}]
		290	(β: 292) [A_{1g}]		(114) [B_{3g}]		(72) [E_g]
		337	(α: 334) [Ag]	168	(175) [B_{1g}]		(74) [B_{2g}]
		410	(α: 385) [B_{3g}]	203	(203) [A_g]		(76) [A_{1g}]
		416	(α: 388) [B_{2g}]	374	(362) [B_{3g}]	92	(85) [E_g]
				585	(606) [B_{1g}]		(88) [B_{2g}]
							(92) [E_g]
						109	(102) [Eg]
							(103) [B_{1g}]
							(109) [B_{2g}]
							(111) [E_g]
							(112) [E_g]
							(118) [A_{1g}]
						131	(132) [B_{1g}]
							(136) [E_g]
							(143) [A_{1g}]
						140	(147) [E_g]
							(148) [B_{2g}]
						368	(350) [B_{2g}]
							(351) [E_g]
						430	(416) [E_g]
						447	(441) [B_{2g}]
						473	(485) [A_{1g}]
							(486) [B_{2g}]
							(491) [B_{1g}]

Table 2 Calculated IR and Raman vibrational modes for BeF_2.

$\alpha-BeF_2$, IR active modes		
wavenumber / cm^{-1}	irreducible representation	intensity / km mol^{-1}
90	E	0
187	E	0
280	A_2	16
302	E	3
388	E	303
412	A_2	181
596	E	3
745	A_2	1354
747	E	2645
793	E	3
831	A_2	6
866	E	53
$\alpha-BeF_2$, Raman active modes		
wavenumber / cm^{-1}	irreducible representation	intensity / a.u.
90	E	91
130	A_1	262
187	E	47
302	E	78
317	A_1	1000
355	A_1	621
388	E	172
596	E	62
746	A_1	33
747	E	42
793	E	3
866	E	31
$\beta-BeF_2$, IR active modes		
wavenumber / cm^{-1}	irreducible representation	intensity / km mol^{-1}
66	E_1	0
380	E_1	321
393	A_2	228
754	E_1	2714
756	A_2	1352
792	E_1	0
$\beta-BeF_2$, Raman active modes		
wavenumber / cm^{-1}	irreducible representation	intensity / a.u.
66	E_1	58
180	E_2	30
295	E_2	16
316	A_1	1000
380	E_1	101
602	E_2	58
754	E_1	14
792	E_1	3
875	E_2	6

Table 3 Calculated IR and Raman vibrational modes for $\alpha-BeCl_2$.

$\alpha-BeCl_2$, IR active modes		
wavenumber / cm^{-1}	irreducible representation	intensity / km mol^{-1}
170	B_{2u}	0
170	B_{3u}	0
449	B_{1u}	1228
560	B_{3u}	402
572	B_{2u}	385
$\alpha-BeCl_2$, Raman active modes		
wavenumber / cm^{-1}	irreducible representation	intensity / a.u.
62	B_{1g}	0
150	A_g	276
169	B_{3g}	189
175	B_{2g}	201
293	B_{1g}	355
334	A_g	1000
385	B_{3g}	71
388	B_{2g}	60
684	B_{1g}	38

Table 4 Calculated IR and Raman vibrational modes for $\beta-BeCl_2$.

$\beta-BeCl_2$, IR active modes		
wavenumber / cm^{-1}	irreducible representation	intensity / km mol^{-1}
57	E_u	0
83	E_u	0
89	E_u	0
108	E_u	1
129	A_{2u}	2
138	A_{2u}	0
153	E_u	6
176	A_{2u}	27
179	E_u	13
197	E_u	5
215	E_u	21
226	E_u	12
227	A_{2u}	14
232	E_u	2
296	E_u	1
328	E_u	16
329	A_{2u}	2
429	E_u	32
434	E_u	5
451	A_{2u}	5577
462	E_u	7503
556	A_{2u}	2
563	E_u	2432
563	E_u	1742
569	A_{2u}	825
588	E_u	60
$\beta-BeCl_2$, Raman active modes		
wavenumber / cm^{-1}	irreducible representation	intensity / a.u.
36	B_{2g}	4
41	E_g	0
46	E_g	14
80	A_{1g}	10
81	E_g	2
88	E_g	5
89	B_{1g}	6
109	E_g	6
123	B_{2g}	0
137	A_{1g}	99
139	B_{1g}	97
142	B_{2g}	10
146	A_{1g}	52
150	E_g	118
175	B_{1g}	0
179	E_g	58
180	B_{2g}	206
199	E_g	2
215	E_g	152
216	B_{1g}	29
226	B_{2g}	10
228	E_g	0
232	E_g	7
245	A_{1g}	85
291	B_{1g}	19
292	A_{1g}	1000
296	E_g	41
327	E_g	15
330	B_{2g}	8
430	E_g	1
432	E_g	0
446	A_{1g}	2
453	B_{2g}	99
462	E_g	73
555	B_{2g}	5
558	E_g	6
559	A_{1g}	11
560	E_g	4
565	B_{1g}	3
572	B_{1g}	5
593	B_{1g}	10
605	E_g	60
608	B_{2g}	6
610	A_{1g}	220

Table 5 Calculated IR and Raman vibrational modes for $BeBr_2$.

$BeBr_2$, IR active modes		
wavenumber / cm^{-1}	irreducible representation	intensity / km mol^{-1}
108	B_{2u}	0
109	B_{3u}	0
400	B_{1u}	1160
492	B_{2u}	349
505	B_{3u}	347
$BeBr_2$, Raman active modes		
wavenumber / cm^{-1}	irreducible representation	intensity / a.u.
45	B_{1g}	0
99	A_g	336
111	B_{2g}	220
114	B_{3g}	239
175	B_{1g}	399
203	A_g	1000
358	B_{2g}	215
362	B_{3g}	220
606	B_{1g}	23

Table 6 Calculated IR and Raman vibrational modes for $\alpha-BeI_2$.

$\alpha-BeI_2$, IR active modes		
wavenumber / cm^{-1}	irreducible representation	intensity / km mol^{-1}
83	B_{2u}	0
87	B_{3u}	0
365	B_{1u}	1181
435	B_{2u}	360
454	B_{3u}	351
$\alpha-BeI_2$, Raman active modes		
wavenumber / cm^{-1}	irreducible representation	intensity / a.u.
51	B_{1g}	1
82	B_{2g}	263
87	A_g	433
88	B_{3g}	309
119	B_{1g}	497
147	A_g	1000
340	B_{2g}	241
343	B_{3g}	217
519	B_{1g}	20

Table 7 Calculated IR and Raman vibrational modes for $\beta-BeI_2$.

$\beta-BeI_2$, IR active modes		
wavenumber / cm^{-1}	irreducible representation	intensity / km mol^{-1}
41	E_u	0
47	E_u	0
53	E_u	0
58	E_u	0
68	A_{2u}	0
71	A_{2u}	0
78	E_u	0
83	A_{2u}	0
84	E_u	1
93	E_u	0
103	E_u	1
108	E_u	8
109	A_{2u}	6
113	E_u	0
136	E_u	1
148	A_{2u}	0
148	E_u	2
349	A_{2u}	3926
351	E_u	4080
372	E_u	271
376	E_u	28
427	E_u	842
451	A_{2u}	157
456	E_u	204
462	E_u	4306
463	A_{2u}	1624
$\beta-BeI_2$, Raman active modes		
wavenumber / cm^{-1}	irreducible representation	intensity / a.u.
29	E_g	0
37	B_{2g}	1
39	E_g	8
46	E_g	0
46	A_{1g}	42
53	E_g	8
56	E_g	12
58	B_{2g}	5
59	B_{1g}	7
66	A_{1g}	154
68	B_{1g}	244
72	E_g	275
74	B_{2g}	8
76	A_{1g}	93
85	B_{1g}	0
85	E_g	149
88	B_{2g}	428
93	E_g	3
102	E_g	334
103	B_{1g}	57
109	B_{2g}	19
111	E_g	1
112	E_g	15
118	A_{1g}	85
132	B_{1g}	53
136	E_g	100
143	A_{1g}	1000
147	E_g	170
148	B_{2g}	54
350	B_{2g}	222
351	E_g	176
372	E_g	0
375	E_g	42
379	A_{1g}	2
416	E_g	65
419	B_{1g}	0
441	B_{2g}	41
447	E_g	5
458	A_{1g}	8
462	B_{1g}	28
471	E_g	4
485	A_{1g}	87
486	B_{2g}	37
491	B_{1g}	106

Table 8 Optimized and experimental[5,12,13] (in brackets) lattice parameters in Å and cell volumes in Å^3.

compound	*a*	*b*	*c*	*V* per formula unit
$\alpha-BeF_2$	4.821 (4.7390(5))		5.294 (5.1875(8))	53.27 (50.45(3))
$\beta-BeF_2$	4.910 (4.8060(1))		5.407 (5.2404(1))	56.45 (52.41(0))
$\alpha-BeCl_2$	5.305 (5.285(3))	10.309 (9.807(3))	5.336 (5.227(3))	72.95 (67.7(2))
$\beta-BeCl_2$	10.883 (10.595(5))		18.457 (18.036(7))	68.31 (63(2))
$BeBr_2$	5.621 (5.569(4))	10.662 (10.405(6))	5.601 (5.543(3))	83.91 (80.3(3))
$\alpha-BeI_2$	5.867 (6.025(3))	11.494 (11.316(4))	5.994 (6.035(3))	101.05 (102.9(3))
$\beta-BeI_2$	11.962 (12.190(6))		21.796 (21.325(8))	97.46 (99(3))

Notes and references

1 STOE WinXPOW, Stoe & Cie GmbH, Darmstadt, Germany, 2011.

2 V. Petricek, M. Dusek, L. Palatinus, Jana 2006 – The Crystallographic Computing System, Institute of Physics, Praha, Czech Republic, 2013.

3 R. E. Rundle and P. H. Lewis, *J. Chem. Phys.*, 1952, **20**, 132–134.

4 E. Spundflasche, H. Fink and H. Seifert, *Z. Anorg. Allg. Chem.*, 1995, **621**, 1723–1726.

5 S. I. Trojanov, *Zh. neorg. Khim.*, 2000, **45**, 1619–1624.

6 OPUS, BRUKER OPTIK GMBH, Ettlingen, Germany, 2009.

7 OriginPro 8, ORIGINLAB, Northampton, MA, USA, 2007.

8 J. Baima, A. Erba, M. Rérat, R. Orlando and R. Dovesi, *J. Phys. Chem. C*, 2013, **117**, 12864–12872.

9 K. Doll and H. Stoll, *Phys. Rev. B*, 1998, **57**, 4327.

10 E. Apra, M. Causa, M. Prencipe, R. Dovesi and V. Saunders, *J. Phys.: Condens. Matter*, 1993, **5**, 2969.

11 R. Nada, C. Catlow, C. Pisani and R. Orlando, *Modell. Simul. Mater. Sci. Eng.*, 1993, **1**, 165.

12 P. Ghalsasi and P. S. Ghalsasi, *Inorg. Chem.*, 2011, **50**, 86–89.

13 A. F. Wright and A. N. Fitch, *J. Solid State Chem.*, 1988, **73**, 298–304.